Materials Advances

ROYAL SOCIETY OF CHEMISTRY

PAPER

View Article Online
View Journal | View Issue

Cite this: *Mater. Adv.*, 2022, 3, 4851

Fused filament fabrication of PVDF films for piezoelectric sensing and energy harvesting applications†

Rui Tao, [a] Jiahao Shi,[b] Mohammad Rafiee,[a] Abdolhamid Akbarzadeh [bc] and Daniel Therriault *[a]

Received 23rd January 2022,
Accepted 29th April 2022

DOI: 10.1039/d2ma00072e

rsc.li/materials-advances

Fused filament fabrication (FFF) of piezoelectric polymer polyvinylidene fluoride (PVDF) provides a simple manufacturing technique for the fabrication of lead-free piezoelectric devices compared to the traditional manufacturing methods, such as large-scale film extrusion and solution casting. Here, we investigate the effects of the stretching and poling parameters on the enhancement of piezoelectric performance of the printed PVDF films. The stretched and polarized PVDF films with dimensions of 40 × 20 × 0.06 mm (length × width × thickness) possess a piezoelectric charge coefficient (d_{33}) of 7.29 pC N^{-1} and a fraction of β phase (F_β) of 65% at a stretching ratio (R) of 4 after being polarized under an electric field of 30 V μm^{-1}. The resulting d_{33} of the fabricated PVDF films has been substantially enhanced by ~10–100 times higher than the related reported values of the FFF printed PVDF films. The fabricated PVDF films are capable of detecting compression (d_{33}) and vibration (d_{31}). By blowing four piezoelectric films connected in parallel for 3 min, the energy stored in the capacitor can make a LED blink. Our fabricated piezoelectric PVDF films could be used in the field of pressure sensing, vibration sensing and energy harvesting applications.

1. Introduction

Piezoelectric materials are used in various applications such as in pressure sensing,[1,2] strain sensing,[3,4] actuation[5,6] and energy harvesting[7,8] because of their capabilities of converting mechanical energy to electrical energy and *vice versa*.[9,10] Compared to high piezoelectric ceramics such as lead zirconate titanate (PZT) and barium titanate ($BaTiO_3$), piezoelectric polymer polyvinylidene fluoride (PVDF) has been increasingly used owing to its lightness, high flexibility, durability and biocompatibility.[11,12] PVDF is a semicrystalline polymer with a repeating unit of the CH_2–CF_2 monomer.[13] It has two main phases: a non-polar α phase and a polar β phase.[14,15] The dipole moments in PVDF originate from the high electronegativity of fluorine atoms and smaller electronegativity of hydrogen atoms.[16,17] The α phase with a *trans*–gauche–*trans*–gauche' (TGTG') conformation is not piezoelectric as a result of the cancellation of the dipole moments, while the β phase with an all trans (TTTT) conformation possesses the largest polarization due to the alignment of the dipole moments in the same direction.[18] However, PVDF usually crystallizes into the thermally stable α phase.[19,20] Several methods have been used to induce the conversion from the α phase to the β phase such as mechanical stretching[21–23] and hot-pressing.[24,25] In addition to the requirement of the high content of the β phase (F_β) in PVDF, an electrical poling treatment is often essential to align the randomly dispersed β phase in order to obtain a net polarization.[26–29] Poling parameters (*e.g.* time, temperature and poling voltage) have to be appropriately adjusted in order to maximize the efficiency of the poling process.[30,31] A high F_β is a prerequisite for achieving a high piezoelectric coefficient of the polarized PVDF elements. The piezoelectric strain coefficient (d_{31} and d_{33}) with double subscripts is used to illustrate the piezoelectric performance: the first subscript indicates the direction of the charge generation and the second subscript indicates the direction of the applied mechanical strain.

Over the past decade, additive manufacturing technology (or 3D printing) has increasingly been utilized to fabricate smart materials including piezoelectric materials.[1,2,32–39] The traditional manufacturing methods for the preparation of PVDF

[a] *Laboratory for Multiscale Mechanics (LM²), Department of Mechanical Engineering, Research Center for High Performance Polymer and Composite Systems (CREPEC), Polytechnique Montreal, Montreal, QC, H3T 1J4, Canada. E-mail: daniel.therriault@polymtl.ca*
[b] *AM³L Laboratory, Department of Bioresource Engineering, McGill University, Montreal, QC, H9X 3V9, Canada*
[c] *Department of Mechanical Engineering, McGill University, Montreal, QC, H3A 0C3, Canada*

† Electronic supplementary information (ESI) available. See DOI: https://doi.org/10.1039/d2ma00072e

films such as solution casting[40–42] and electrospinning[43–45] require toxic solvents, while extrusion molding[19,42] requires careful control of the melt temperature and the material feeding rate. Thus, fused filament fabrication (FFF) offers a maneuverable and eco-friendly approach for the fabrication of piezoelectric PVDF devices, *i.e.*, recyclable and without the requirement of a toxic solvent. Several studies demonstrated FFF 3D printing of piezoelectric PVDF films. Lee *et al.*[35] and Kim *et al.*[33] integrated FFF 3D printing and electrical poling steps to achieve one-step fabrication of piezoelectric PVDF films. Porter *et al.*[32] investigated the effects of printing parameters on the piezoelectric performance of the PVDF films. However, the reported piezoelectric coefficients in these studies (Kim *et al.*:[33] d_{33} = 0.048 pC N^{-1}; Porter *et al.*:[32] d_{31} = 1.19 pC N^{-1}) are much lower than those of the commercial hot-pressed piezoelectric PVDF films, which are in the range of 28–32 pC N^{-1}.[46] In addition, some researchers incorporated fillers to induce the generation of β phases in the FFF 3D printed PVDF films. Pei *et al.*[47] added 5 wt% tetraphenylphosphonium chloride (TPPC) nanoparticles to obtain 83.8% β phases, while 28.9% of the β phase content for pure PVDF. Liu *et al.*[48] enhanced the β phase content of the PVDF filament to 93% by adding 15 wt% ionic liquid as compared to only 13.5% of the β phase in pure PVDF.

Our novel strategy in this work is to fabricate piezoelectric PVDF films with highly enhanced d_{33} compared to the related reported values[33] using the facile FFF 3D printing technique and two tailored post-treatments: mechanical stretching and electrical poling. Four different stretching ratios (R = final length/original length, R = 1, 2, 3 and 4) are investigated to achieve the highly polar β phase content. We then used the polarized printed piezoelectric PVDF films in three applications: a frequency detector, a pressure sensor and energy harvesters to convert wind energy to electricity. We believe that FFF 3D printing technology with appropriate post-treatments investigated herein is promising for the construction of flexible PVDF piezoelectric sensors and energy harvesters for more advanced applications in areas ranging from medical to aerospace and beyond.

2. Experimental section

Materials

PVDF filaments (1.75 mm in diameter, Fluorinar-H™ Kynar®) were purchased from Nile Polymers, Inc (USA). Commercially available unpolarized (R = 5) and polarized (R = 5) hot-pressed PVDF films with a thickness of ~120 μm were purchased from PolyK Technologies, LLC (USA).

FFF printing of PVDF films

PVDF films were fabricated using a commercially available 1.75 mm diameter PVDF filament. An FFF 3D printer (Raised3D Pro 2) was used to print a one-layer film with dimensions of 60 × 40 × 0.15 mm. Table 1 lists the main printing parameters.

Table 1 FFF 3D printing parameters for preparing the PVDF films

Parameters	Values
Nozzle size	0.4 mm
Bed temperature	100 °C
Extrusion temperature	250 °C
Printing speed	30 mm s^{-1}
Infill percentage	100%
Layer height	0.15 mm

Stretching process

The stretching process was carried out on the printed PVDF films using a tensile test machine (eXpert 2600, ADMET). The dimensions of the PVDF film between the upper and lower grips were 40 × 40 × 0.15 mm. The stretching conditions were 100 °C in an environmental chamber (F-280DT, ADMET) and a stretching rate of 0.2 mm s^{-1}. When other temperatures (80 to 120 °C) and speed (0.1 to 1 mm s^{-1}) settings were used, the PVDF films cracked during the stretching process. The stretching ratios were varied from 1 to 4. The PVDF films have a great tendency to crack during the stretching process if we stretch them with $R > 4$.

Poling process

We built a contact poling setup to align the dipole moments of PVDF films, which consisted of three parts: an in-house-designed poling chamber, a high voltage power supply (ES60kV negative, 10 Watt, Gamma High Voltage Research, Inc.) and a hot plate (Thermo Scientific™ SuperNuova + ™, Fisher Scientific). (see Fig. S1, ESI†) The commercially available hot-pressed PVDF films were polarized to confirm the functionality of the in-house built poling setup.

Before the poling process, both the 3D printed and commercial PVDF films were cut into the same size of 40 × 20 mm and attached with conductive aluminum tape (3M, USA) to both surfaces as poling electrodes. During the poling process, the specimen was clamped between the copper rod and the bottom aluminum plate. Then, the specimen was cooled down to room temperature before removing the electric field to reduce the misalignment of dipole moments. After the poling process, the aluminum tapes were removed, and the films were washed with soap to remove the residue of silicone oil and dried at room temperature before painting the electrodes on their top and bottom surfaces.

To evaluate the poling performance of the contact poling setup, unpolarized commercially stretched hot-pressed PVDF films are polarized using four poling voltages (2, 4, 6 and 8 kV) at 80 °C for 60 min, four poling times (30, 60, 90 and 120 min) at 80 °C under 6 kV and five poling temperatures (room temperature, 50, 80, 110 and 140 °C) under 6 kV for 60 min, respectively. To investigate the optimal poling conditions for the printed PVDF films stretched at R = 4 (highest F_β), we further polarized them using three poling voltages (1, 2 and 3 kV) at 80 °C for 60 min, four poling times (30, 60, 90 and 120 min) at 80 °C under 2 kV and five poling temperatures (room temperature, 50, 80, 110 and 140 °C) under 2 kV for 60 min, respectively. In addition, the printed PVDF films stretched at R = 1, 2 and 3 are also polarized with an electric field of 30 V μm^{-1} at 80 °C for 60 min.

Electrode fabrication and electrical connection process

A bristle paintbrush was used to paint a thin layer of silver conductive paste (MG Chemicals 842AR, ABRA Electronics Corp.)

on the top and bottom surfaces of the printed piezoelectric PVDF films as electrodes for the electromechanical measurement. We left a gap (~2 mm) between the edge of the silver electrodes and the edge of the PVDF films in order to avoid contact between the two electrodes. Then, two pieces of aluminum tapes (5 × 10 mm) were used to electrically connect the silver electrodes and the wires.

Piezoelectric property characterization

A d_{33} meter (YE2730, Sinocera Piezotronics, Inc.) was used to characterize the piezoelectric coefficient d_{33}. The specimens were tested approximately one day after the poling process because the d_{33} value measured immediately after the poling process is higher than the real value. In the cantilever bending and compression tests, open-circuit voltages were collected using a charge amplifier (Piezo Lab Amplifier, MEAS Specialties) in the voltage mode. The data were acquired with an NI-9239 data acquisition system attached to a USB carrier NI-9162 (National Instruments) and recorded using a custom LabVIEW interface.

Piezoelectric β phase characterization

A Fourier-transform infrared (FTIR) spectrometer (Nicolet 6700, Thermo Scientific) was used to obtain the absorption spectra of different types of PVDF films at 8 cm^{-1} resolution from 550 to 1250 cm^{-1}. 128 scans were conducted on each sample and the average values were used to assess the content of different phases.

Optical characterization

A Canon EOS Rebel T4i camera was used for the photography of the samples in this paper. Optical images of the cross-section of the sensors (Fig. 1f) were taken using an optical microscope (BX-61, Olympus). A high-speed camera (MotionBLITZ Cube4, Mikrotron) captured the cantilever bending test at a frame rate of 200 Hz.

Cantilever bending test

An aluminum beam with dimensions of 120 × 40 × 0.5 mm was fixed on a steel support and bent dynamically by a shaker (K2004E01, Mode Shop Inc.). The span length is ~8 cm. The printed piezoelectric PVDF films were attached near the clamped end of the aluminum beam in order to exhibit maximum strain and detect the vibration frequency. During the cantilever bending test, the shaker was excited by a function generator (Model 19, Wavetek Corp.) in a sine wave format at eight different frequencies: 0.1, 0.5, 1, 5, 10, 20, 30 and 40 Hz.

Compression test

Compression tests of the printed piezoelectric PVDF films were carried out on an MTS Insight machine with a 1000 N load cell in the compression mode (MTS 569332-01). The crosshead speed was 1 mm s^{-1}. An acrylic disc with a diameter of 10 mm was glued on top of the PVDF film to obtain the same contact area under compression. The compression head moved down 0.033, 0.056, 0.079, 0.101, 0.129, 0.159, 0.206 and 0.234 mm until the maximum compressive force of 100, 200, 300, 400, 500, 600, 700 and 800 N was reached, respectively. The average voltage output is calculated from three measurements.

Energy harvester

Four FFF printed PVDF films were connected in parallel and glued on a 3D printed PLA tree as the energy harvesting

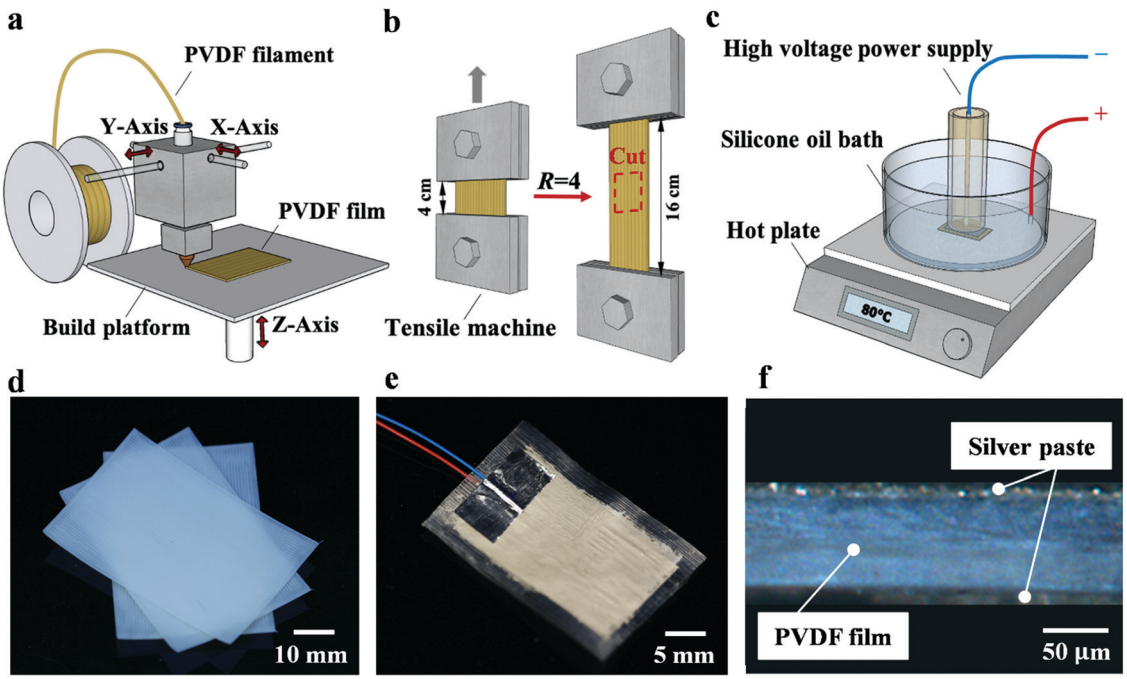

Fig. 1 Fabrication of the piezoelectric PVDF films. Schematic of the (a) FFF printing process of the PVDF films (60 × 40 × 0.15 mm). (b) Stretching process of the printed PVDF films (R = 4). (c) Contact poling process of the stretched PVDF films (40 × 20 × 0.06 mm). Photos of (d) FFF printed PVDF films. (e) A piezoelectric PVDF film with electrical connections. (f) Optical image of the cross-section of the piezoelectric PVDF film.

"leaves" and blown using a tabletop air circulation fan (PFT30T2ABB-V, PELONIS) at 1500 rpm. A circuit was built in order to light a red LED using the energy generated by the "piezo leaves". In this circuit, a bridge-rectifier consisting of four diodes converted the AC generated by these four "piezo leaves" to DC, while a 2.2 μF capacitor stored the converted energy. The stored voltage in the capacitor was displayed on a digital multimeter (HHM11, Omega Engineering, Inc.).

3. Results and discussion

Fig. 1a–c schematically shows the fabrication process of a piezoelectric PVDF film based on FFF printing, stretching (R = 4) and poling processes. The FFF printed one-layer PVDF films are stretched along with the printing direction at R = 4 (*i.e.*, from 4 cm to 16 cm) to induce the generation of the β phase (Fig. 1a and b). Then, the stretched PVDF films are cut to 40 × 20 mm and polarized along the thickness direction by a contact poling setup to align the randomly oriented dipole moment (Fig. 1c). Fig. 1d shows the photo of the printed PVDF films (60 × 40 × 0.15 mm). For efficient performance, the FFF printed PVDF films have to be free of porosities or impurities, otherwise a premature breakage during the mechanical stretching process or a permanent electrical breakdown during the poling process could happen. In case of an electrical breakdown, the piezoelectric element could not be further polarized and the piezoelectricity will remain very low. Undesired porosities or impurities can be created during the filament preparation and/or the FFF printing process. First, the as-received printing filament should have the least content of bubbles and impurities. Second, the PVDF filaments were dried in the oven to minimize their moisture content and the pores in the printed parts.

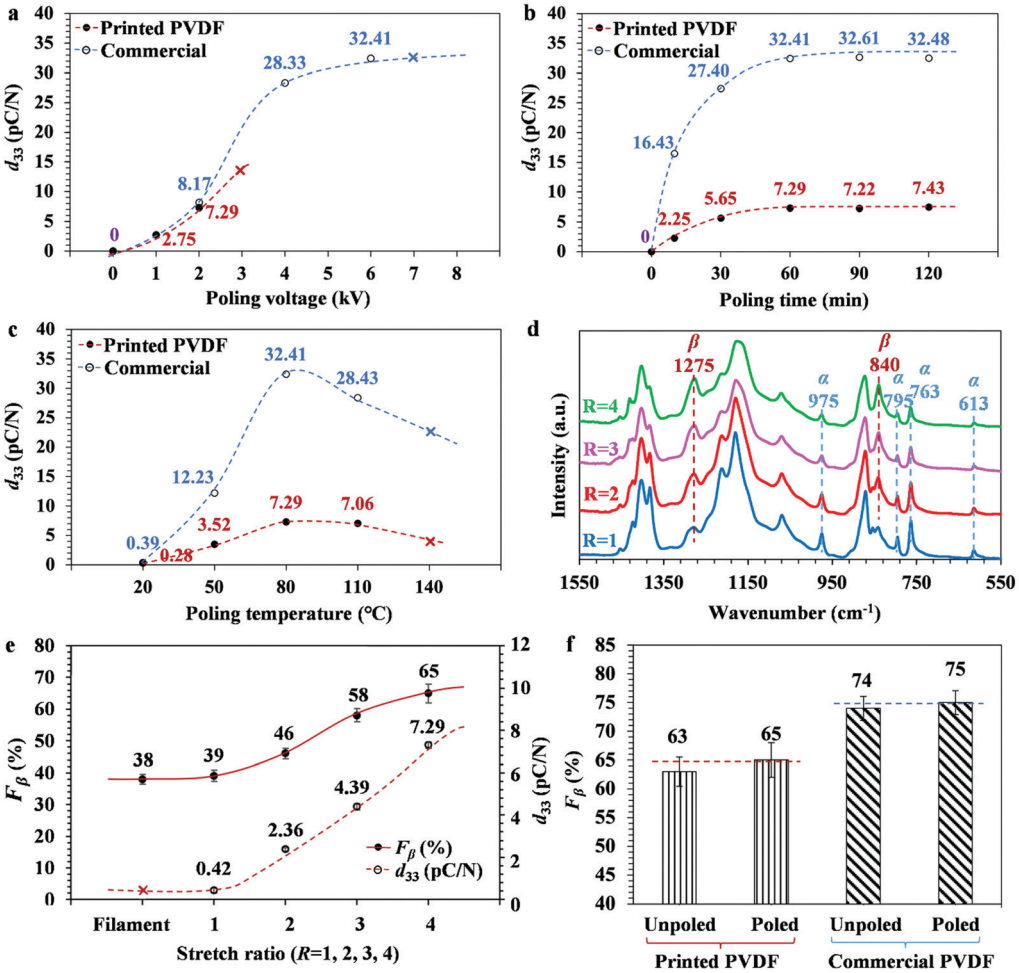

Fig. 2 Investigation of the optimal poling and stretching parameters by characterizing and comparing the piezoelectric behaviors of printed PVDF films fabricated in this work and stretched commercial hot-pressed PVDF films. (a) d_{33} of commercial and printed (R = 4) PVDF films polarized under different poling voltages: 2, 4, 6 and 7 kV (for commercial PVDF); 1, 2 and 3 kV (for printed PVDF) (red and blue markers represent electrical breakdown). (b) d_{33} of commercial and printed (R = 4) PVDF films polarized for different poling times: 30, 60, 90 and 120 min. (c) d_{33} of commercial and printed (R = 4) PVDF films polarized at different poling temperatures: room temperature, 50, 80, 110 and 140 °C (red and blue markers represent electrical breakdown). (d) FTIR spectrum, (e) F_β (%) and d_{33} of the unprinted PVDF filament and polarized printed PVDF films stretched at R = 1, 2, 3 and 4. (poling parameters: 80 °C, 30 V μm^{-1} and 60 min) (f) Comparison of F_β (%) of printed PVDF films fabricated in this work (R = 4) and commercial PVDF films before and after the poling process.

Meanwhile, we slightly increase the extrusion width to make sure there is no gap between the printed lines (Fig. S2, ESI†). A fabricated PVDF film with electrical connections is shown in Fig. 1e. The optical image of the cross-section of the piezoelectric PVDF film with electrodes shown in Fig. 1f illustrates that the average thickness of the piezoelectric PVDF film after being stretched at R = 4 is ~60 μm and the average thickness of the painted silver electrodes on each side is ~15 μm. The photo and the thickness of the PVDF films stretched at R = 1, 2 and 3 are shown in Fig. S3 and listed in Table S1 in the ESI.†

Poling voltage, time and temperature are the three main poling parameters that influence the piezoelectric properties of polarized PVDF films. Poling voltage should be sufficiently high to align the dipole moments, while poling time should be optimized to ensure complete polarization in the shortest time. An elevated poling temperature is used to increase the mobility of the PVDF molecules. Fig. 2a–c show the d_{33} of the printed PVDF films (R = 4) and the commercial unpolarized PVDF films with respect to poling voltage, time and temperature, respectively. In Fig. 2a, d_{33} values of both printed (R = 4) and commercial PVDF films increase rapidly and then reach a plateau value with the enhancement of the poling voltage (poling temperature = 80 °C and poling time = 60 min). For the commercial stretched PVDF films, under the highest poling voltage value of 6 kV, which is approximately 50 V μm^{-1} electric field, the maximum d_{33} value of 32.41 pC N^{-1} is reached, consistent with the reported d_{33} value (32 pC N^{-1}) of the commercial polarized PVDF film measured using a d_{33} meter.[46] Electrical breakdown occurs at ~7 kV as marked in blue. The printed PVDF films (R = 4) can hold a maximum poling voltage of 2 kV, which is approximately 30 V μm^{-1} electric field and leads to a maximum d_{33} value of 7.29 pC N^{-1}. Electrical breakdown of the PVDF film occurs at 3 kV as marked in red. The maximum poling electric field of the printed PVDF films (R = 4) is less than those of commercial PVDF films due to the fact that the thinner section is present between the extruded lines in the printed PVDF films (Fig. S2, ESI†). In Fig. 2b, d_{33} of both printed (R = 4) and commercial PVDF films increase rapidly and then reach a plateau value with the poling time (poling temperature = 80 °C, poling voltage = 50 V μm^{-1} (commercial PVDF) and 30 V μm^{-1} (printed PVDF)). For both commercial and printed PVDF films, the d_{33} value increases with poling time until 60 min. The d_{33} is almost constant for a poling time beyond 60 min probably due to the completion of the alignment of the dipole moments in that period. In Fig. 2c, d_{33} of both printed (R = 4) and commercial PVDF films increase until 80 °C and then drop down with the increase of poling temperature (poling time = 60 min, poling voltage = 50 V μm^{-1} (commercial PVDF) and 30 V μm^{-1} (printed PVDF)). We observe that the highest d_{33} value is achieved at 80 °C. Below 80 °C, the PVDF molecules are inactive, so it could not be reoriented efficiently along with the electric field.[49] However, when the poling temperature is above 80 °C, we observed that the PVDF films significantly warp and detach from the bottom poling plate, so the poling electric field cannot be uniformly applied on the PVDF films. The investigation of the poling parameters for the commercial PVDF films suggests that the optimal poling settings are 80 °C, 50 V μm^{-1} and 60 min. However, the printed PVDF films could not sustain more than 30 V μm^{-1} because of the thinner area between printed lines. Thus, the tailored poling settings for the printed PVDF films are 80 °C, 30 V μm^{-1} and 60 min. In the d_{33} measurement, three specimens are tested and each specimen is measured at three different locations. We found that the error bar of the specimens polarized under the same conditions is too small to be detected, which indicates the PVDF films have been uniformly polarized.

We investigate the effect of R on the generation of piezoelectric β phases in the printed PVDF films. The photos and the dimensions of the printed PVDF films stretched at R = 1, 2, 3 and 4 are shown in Fig. S3, ESI.† The FTIR spectra of the polarized printed PVDF films stretched at R = 1 to 4 are shown in Fig. 2d. Herein, 840 cm^{-1} is the characteristic peak of the piezoelectric β phase, while 613, 713, 795 and 975 cm^{-1} are the representative peaks of the piezoelectric α phase. With the increase of R, the peaks of the α phase decrease, while the peak of the β phase increases, meaning that the printed PVDF films transform from the α phase into the β phase. For a system containing α and β phases, the modified Beer–Lambert law is used to calculate F_β (%):

$$F_\beta(\%) = \frac{A_\beta}{1.26A_\alpha + A_\beta} \quad (1)$$

where A_α and A_β are the absorbance of α and β phases at 763 and 840 cm^{-1}, respectively, and 1.26 is the ratio of the absorption coefficient at the corresponding wavenumber of 6.1 × 10^4 and 7.7 × 10^4 cm^2 mol^{-1} for α and β phases, respectively.[19,50] Three specimens are prepared for each stretching condition and F_β (%) and d_{33} of each specimen is measured at three different locations. As shown in Fig. 2e, F_β (%) and d_{33} increase with the value of R. The unprinted PVDF filament and the printed PVDF films stretched at R = 1 have a similar low F_β (%) and d_{33}, indicating that the 3D printing process cannot efficiently convert the α phase to β phase in PVDF. Both F_β (%) and d_{33} increase with R, which means that the stretching process is necessary for achieving higher piezoelectric performance. The polarized printed PVDF films possess an F_β (%) of 65% and a d_{33} of 7.29 pC N^{-1}, which is ~10–100 times higher compared to the previously reported FFF 3D printed PVDF films (Kim *et al.*:[33] d_{33} = 0.048 pC N^{-1}; Porter *et al.*:[32] d_{31} = 1.19 pC N^{-1}). The commercial hot-pressed PVDF film has a F_β of 74% and a d_{33} of 28 pC N^{-1}. The lower d_{33} of the FFF printed PVDF film compared to the commercial one is due to the lower poling electric field they can reach before the electrical breakdown occurs. The interface between the printed lines, and the surface roughness have an adverse effect during the poling phase. Further optimization of the FFF process parameters (*e.g.*, chamber temperature, nozzle size) might lead to an optimal poling electrical field to reach the performance of commercial dense films. Also, the lower F_β arises from the stretching process, when R > 4, our printed PVDF films rupture, while the commercial films had already been stretched at R = 5. The utilization of a lower R value

is due to the relatively weak interface between the printed lines that makes the printed films fail prematurely. In addition, we compare F_β (%) of the printed PVDF films and the commercial PVDF films before and after the poling process with their respective optimal poling parameters (Fig. 2f). For both PVDF films, F_β (%) has not been much enhanced by the poling step. The commercial PVDF films have a slightly higher F_β (%) than the printed PVDF films owing to the hot-pressing process and the higher R (R = 5) during the stretching process. In conclusion, the stretching process creates higher F_β (%) and poling process aligns β PVDF molecules to achieve a non-zero net polarization. In addition, we heat the polarized printed PVDF films at 30, 40, 50, 60, 70, 80, 90 until 100 °C. Below 60 °C, d_{33} is stable. Above 60 °C, d_{33} decreases with increasing temperature due to the misalignment of the PVDF molecules, *i.e.*, losing their net polarization. Thus, the maximum allowable operating temperature for the FFF printed piezoelectric PVDF films developed in this work is 60 °C as shown in Fig. S4, ESI.†

We chose 40 × 20 × 0.06 mm polarized printed piezoelectric PVDF films (R = 4; polarized at 80 °C, 30 V μm^{-1} for 60 min) for the demonstration of two sensing (cantilever bending – d_{31} mode and compression tests – d_{33} mode) and one energy harvesting applications:

Application #1: cantilever for bending frequency sensing application

A cantilever bending test setup (Fig. 3a) is designed to evaluate the frequency detection behavior of the printed piezoelectric PVDF sensor. The shaker and the aluminum beam are fixed on a steel support and connected to a rod. The screwed rod moves back and forth in the x direction and bends the aluminum beam. The printed piezoelectric PVDF sensor is attached near the clamped end of the aluminum beam. The cantilever bending test was also recorded by the high-speed camera as shown in the ESI.† Movie S1. The shaker is excited by a function generator (in sine wave format) at eight frequencies (*i.e.*, 0.1, 0.5, 1, 5, 10, 20, 30 and 40 Hz) and the deflection of the free end of the aluminum beam is held constant at +5/0 mm. To validate the durability of the printed piezoelectric sensor, we performed the cyclic test at 5 Hz for around 8 h and captured the voltage at the beginning and at the end of the cyclic test for 1200 s, respectively. The printed piezoelectric PVDF sensor still shows good sensitivity and favorable stability for more than 140 000 cycles (Fig. 3b). Fig. 3c shows the voltage generated from the printed piezoelectric film sensor in a period of 1 s between 0.1 and 40 Hz. The measured peak-to-peak voltage is ~0, 9, 39, 35, 29, 6, 2 and 0 mV. The highest peak-to-peak voltage output of ~39 mV is observed at 1 Hz. The peak-to-peak voltage increases from 9 to 39 mV as the frequency increases from 0.5 to 10 Hz and then decreases to 2 mV as the frequency increases from 10 to 30 Hz. The detected frequency by the printed piezoelectric sensor is consistent with the related actuating frequency between 0.5 to 30 Hz. The output voltage signal is close to zero below 0.5 Hz and above 30 Hz. Below 0.5 Hz, the movement is too slow to be detected. The reason is that the piezoelectric sensors are good at dynamic force measurement instead of static force measurement due to the fact that the surface charges are easily neutralized under static force.[51] Above 30 Hz (*i.e.*, frequency = 40 Hz), the piezoelectric PVDF sensor does not have enough time to transmit the charges generated from the bending movement in the positive x direction (forward); these charges are

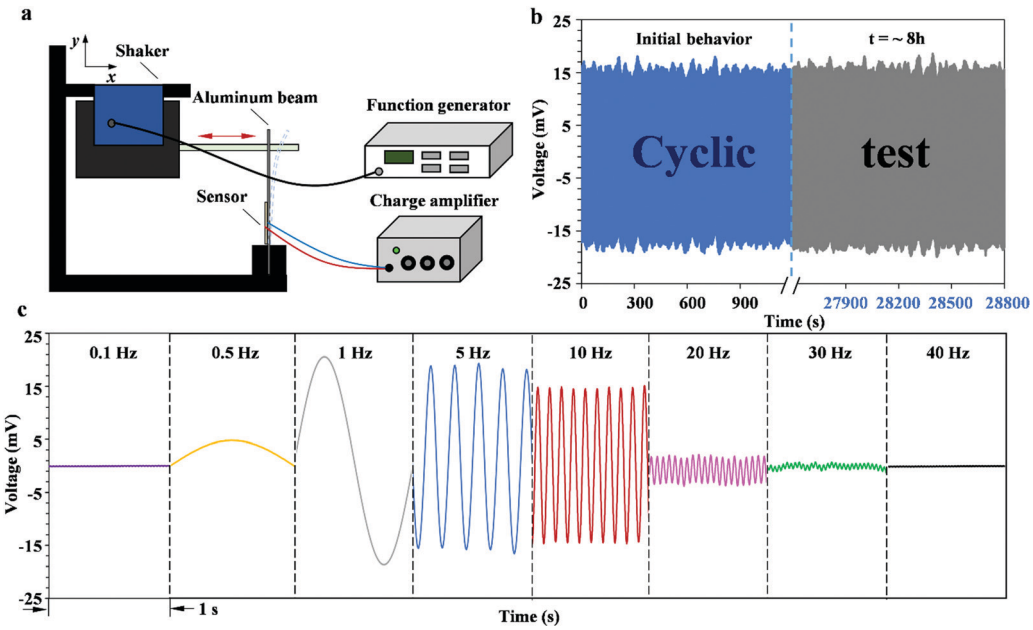

Fig. 3 Cantilever bending test at different frequencies actuated by a shaker. (a) Schematic of the cantilever bending test setup. (b) Durability test for a polarized printed PVDF film sensor (R = 4) by continuous bending at 5 Hz for 144 000 cycles. The voltage generated in 1200 s intervals at the beginning and after 8 h. (c) Voltage generated by a polarized printed piezoelectric PVDF sensor (R = 4) at different actuating frequencies of 0.1, 0.5, 1, 5, 10, 20, 30 and 40 Hz.

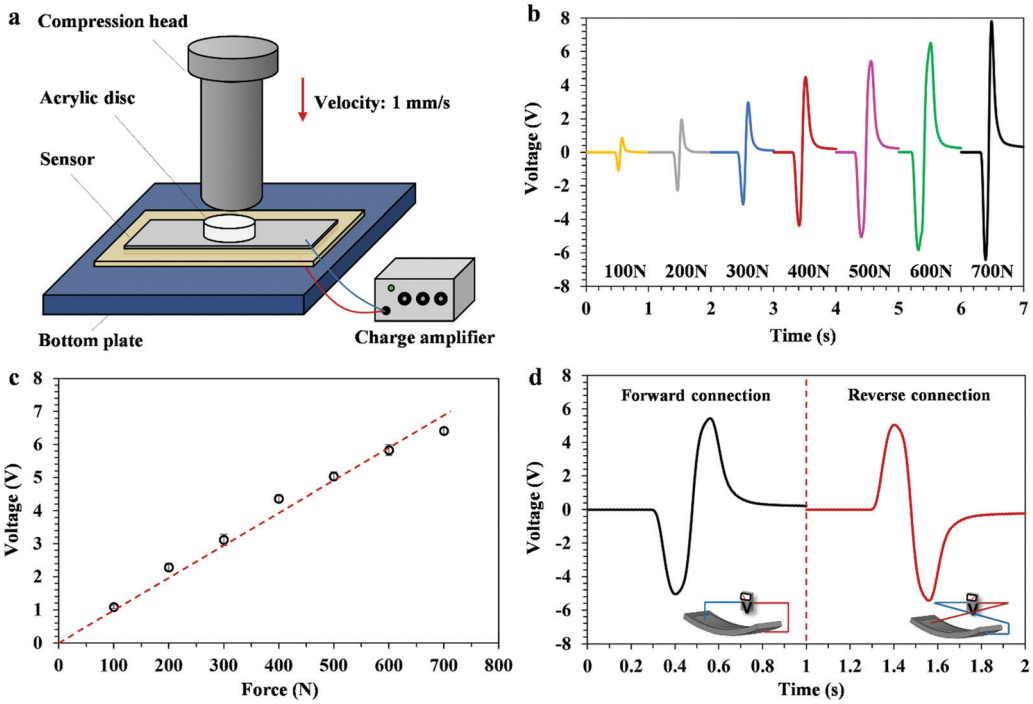

Fig. 4 Compression test. (a) Schematic of the compression test setup. (b) Voltage curves during a 1 s period. (c) Maximum voltage generated by a 40 × 20 mm printed piezoelectric PVDF sensor (R = 4) under the maximum compressive forces of 100, 200, 300, 400, 500, 600 and 700 N. Error bars indicate the standard deviations obtained from three measurements. (d) Switching-polarity test: voltage generated during a 1 s period under the compression of 500 N using forward and reverse connections.

reversed by the recovery movement in the negative x direction (backward).

Application #2: compression sensing application

The schematic of the compression test setup is shown in Fig. 4a. During the test, the compression head goes down by 0.033, 0.056, 0.079, 0.101, 0.129, 0.159, 0.206 and 0.234 mm to reach the maximum compressive force of 100, 200, 300, 400, 500, 600, 700 and 800 N, respectively. The voltage curves of the printed piezoelectric PVDF sensor under the compressive force between 0 to 700 N during a 1 s interval are shown in Fig. 4b. The PVDF films rupture when the load is equal to or greater than 800 N. As the compressive force increases, it takes a longer time for the voltage signal to go back to zero. Fig. 4c depicts a linear response of the PVDF film sensor voltage output for the force range between 0 and ~700 N. The sensitivity of the sensor is ~9.717 mV N^{-1}. Then, we reversed the direction of the connection by switching the positive and negative wires on the piezoelectric sensor, and compressed the piezoelectric sensor with a load of 500 N. We observe that the direction of the voltage peak has been reversed, but the amplitude of two peaks is very close with a 0.8% difference, which confirms that the voltage comes from the piezoelectric sensor and not from the movement of the wires due to the change of the capacitance (Fig. 4d).

Application #3: "piezo leaves" for energy harvesting application

As shown in Fig. 5a, Four 40 × 20 × 0.06 mm printed polarized piezoelectric PVDF sensors (R = 4) are connected in parallel and glued on an FFF 3D printed PLA tree as energy harvesting "piezo leaves". Fig. 5b shows a bridge-rectifier circuit used to convert the AC to DC to charge a 2.2 μF capacitor.[52] In the energy harvesting test, we use a table fan to blow the "piezo leaves" (Fig. 5c). The distance between the fan and the PLA tree is 10 cm. As we turn on the table fan to the highest speed (motor speed = 1500 rpm), the "piezo leaves" are bent, thus generating electric current. We record the voltage reading of the capacitor on the multimeter every 30 sec. During a 3 min period of fan blowing, the "piezo leaves" are able to charge the capacitor from 0 to ~2 V at a charging rate of ~667 mV min^{-1}. After we turn off the fan, the voltage drops gradually due to the intrinsic current leakage behavior of the capacitor (Fig. 5d). A 2.2 μF capacitor is selected in order to balance the current leakage rate and the charging rate. Larger capacitors have a higher charging rate but larger current leakage. The charges stored in the capacitor are further used to make a red LED bulb blink (ESI:† Movie S2). The number of "piezo leaves" and the amplitude of wind power have a significant effect on the charging rate. By calculation, ~720 pieces of "piezo leaves" are required to light a LED continuously.

As shown in Fig. S5 (ESI†), the calculated power density of the four "piezo leaves" is ~9.38 μW cm^{-3} at a resistance of 1 MΩ (although there is a small deformation under the wind), which is comparable to the power density of the PVDF related energy harvesters from other works.[53–55]

4. Conclusion

In summary, we have successfully optimized the stretching–poling post-treatment parameters to fabricate FFF printed

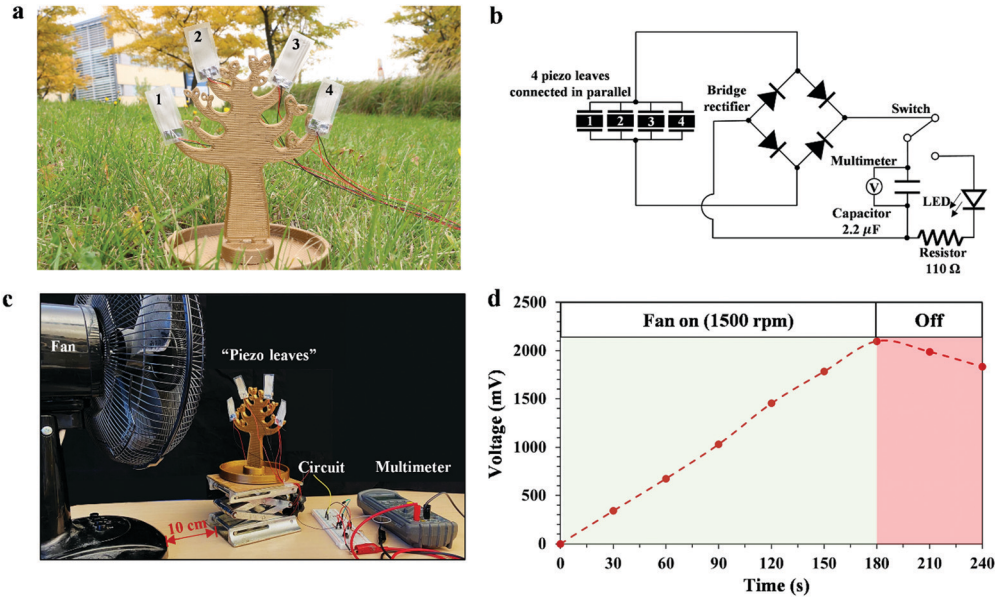

Fig. 5 "Piezo leaves" energy harvester – Four PVDF films connected in parallel blown by a fan. (a) Photo of the four 40 × 20 mm printed piezoelectric PVDF sensors (R = 4) glued on an FFF 3D printed PLA tree. (b) Circuit diagram of the energy harvester: four "piezo leaves" connected in parallel generate AC, which is converted to DC by a bridge rectifier and stored in a capacitor to light a LED bulb. (c) Photo of the experimental setup: the wind energy from the fan is converted to electrical energy by four "piezo leaves" and the stored voltage in an energy harvesting circuit is read by a multimeter. (d) Voltage of a 2.2 μF capacitor charged by the "piezo leaves" after the fan is turned on (1500 rpm) for 3 min and then turned off.

piezoelectric PVDF films and tested them for frequency sensing, pressure sensing and energy harvesting applications. By tailoring the stretching and poling parameters, a piezoelectric coefficient of 7.29 pC N^{-1} and a fraction of β phase of 65% were obtained. We find that the stretching step is necessary for the generation of the piezoelectric β phase, while the poling step is required to align the randomly dispersed dipole moments. The d_{33} of the polarized printed PVDF films (R = 4; polarized at 80 °C, 30 V μm^{-1} for 60 min) fabricated in this work is ~10–100 times higher than the reported values.[32,33] We have successfully demonstrated that the fabricated PVDF films could be directly used in both d_{31} and d_{33} mode sensing applications, including frequency (0.5 to 30 Hz) and compression detection (0 to 700N). Moreover, the 2 V voltage generated and stored in a 2.2 μF capacitor through a 3 min fan blowing of four printed PVDF films connected in parallel could make a LED bulb blink. In future work, to further enhance the piezoelectric charge coefficient of the 3D printed piezoelectric films, high piezoelectric ceramic fillers can be incorporated into the pure PVDF filament as a piezoelectric composite filament. The obtained piezoelectric coefficient will be the sum of the PVDF polymer matrix and the ceramic fillers. In addition, the stretching step is essential to enhance the β phase content in PVDF to achieve better piezoelectric performance, however, it limits the complexity of the manufacturable structures. In our future work, we will show the use of the FFF 3D printing technique to fabricate geometrically optimized true 3D piezoelectric composite devices. The present work is the foundation of our future work with the goal of showing the upper limit of piezoelectric performance that we can achieve in the FFF 3D printed PVDF films. Also, we plan to utilize a multi-material FFF 3D printing technique for the fabrication of piezoelectric sensors with electrodes in a single step. This multi-material 3D printing technique will offer a facile way to create piezoelectric devices without the need for post-metallization. We believe that FFF 3D printed piezoelectric devices would find enormous applications in sensing and energy harvesting fields.

Author contributions

This manuscript was written through contributions from all authors. All authors have given approval to the final version of the manuscript.

Conflicts of interest

There are no conflicts to declare.

Acknowledgements

The authors acknowledge support from the National Science and Engineering Research Council (NSERC), the Discovery program (#RGPIN-4566-2018) and the Department of National Defence (DND) (Grant#: DGDND-2018-00011). Ms Rui Tao and Mr Jiahao Shi acknowledge the financial support received from the China Scholarship Council (CSC). The authors are thankful for the instrument and the lab access kindly provided by Prof. Frédérick Gosselin, Prof. Stéphane Étienne, Prof. Annie Ross, and Prof. Abdellah Ajji at Polytechnique Montreal. The authors would like to especially thank technicians Mr Yanik Landry-Ducharme, Mr Bénédict Besner, Mr Nour Aimene, Mr Robert

Delisle, and research associates Mr Matthieu Gauthier and Mr Richard Silverwood for the technical support, as well as Dr Rouhollah Farahani, Dr Kambiz Chizari and Dr Shibo Zou for technical advice.

References

1 Z. Wang, X. Yuan, J. Yang, Y. Huan, X. Gao, Z. Li, H. Wang and S. Dong, 3D-Printed Flexible, Ag-Coated PNN-PZT Ceramic-Polymer Grid-Composite for Electromechanical Energy Conversion, *Nano Energy*, 2020, **73**(March), 104737.

2 S. Bodkhe, G. Turcot, F. P. Gosselin and D. Therriault, One-Step Solvent Evaporation-Assisted 3D Printing of Piezoelectric PVDF Nanocomposite Structures, *ACS Appl. Mater. Interfaces*, 2017, **9**(24), 20833–20842.

3 X. Lu, H. Qu and M. Skorobogatiy, Piezoelectric Micro- and Nanostructured Fibers Fabricated from Thermoplastic Nanocomposites Using a Fiber Drawing Technique: Comparative Study and Potential Applications, *ACS Nano*, 2017, **11**(2), 2103–2114.

4 Z. Huo, X. Wang, Y. Zhang, B. Wan, W. Wu, J. Xi, Z. Yang, G. Hu, X. Li and C. Pan, High-Performance Sb-Doped p-ZnO NW Films for Self-Powered Piezoelectric Strain Sensors, *Nano Energy*, 2020, **73**(February), 104744.

5 X. Wang, X. He, H. Zhu, L. Sun, W. Fu, X. Wang, L. C. Hoong, H. Wang, Q. Zeng, W. Zhao, J. Wei, Z. Jin, Z. Shen, J. Liu, T. Zhang and Z. Liu, Subatomic Deformation Driven by Vertical Piezoelectricity from CdS Ultrathin Films, *Sci. Adv.*, 2016, **2**(7), 1–10.

6 Y. Wu, J. K. Yim, J. Liang, Z. Shao, M. Qi, J. Zhong, Z. Luo, X. Yan, M. Zhang, X. Wang, R. S. Fearing, R. J. Full and L. Lin, Insect-Scale Fast Moving and Ultrarobust Soft Robot, *Sci. Rob.*, 2019, **4**(32), 1594–1603.

7 N. Li, Z. Yi, Y. Ma, F. Xie, Y. Huang, Y. Tian, X. Dong, Y. Liu, X. Shao, Y. Li, L. Jin, J. Liu, Z. Xu, B. Yang and H. Zhang, Direct Powering a Real Cardiac Pacemaker by Natural Energy of a Heartbeat, *ACS Nano*, 2019, **13**(3), 2822–2830.

8 Y. Zhang, C. R. Bowen, S. K. Ghosh, D. Mandal, H. Khanbareh, M. Arafa and C. Wan, Ferroelectret Materials and Devices for Energy Harvesting Applications, *Nano Energy*, 2019, **57**, 118–140.

9 J. Shi and A. H. Akbarzadeh, Architected Cellular Piezoelectric Metamaterials: Thermo-Electro-Mechanical Properties, *Acta Mater.*, 2019, **163**, 91–121.

10 J. Shi and A. H. Akbarzadeh, 3D Hierarchical Lattice Ferroelectric Metamaterials, *Int. J. Eng. Sci.*, 2020, **149**, 103247.

11 W. Kim, S. Pyo, M. O. Kim, Y. Oh, D. S. Kwon and J. Kim, Humidity-Resistant Triboelectric Energy Harvester Using Electrospun PVDF/PU Nanofibers for Flexibility and Air Permeability, *Nanotechnology*, 2019, **30**(27), 275401.

12 A. S. Fiorillo, S. A. Pullano, M. G. Bianco, C. D. Critello and U. S. Bioinspired, Sensor for Broadband Applications, *Sens. Actuators, A*, 2019, **294**, 148–153.

13 E. Ghafari, X. Jiang and N. Lu, Surface Morphology and Beta-Phase Formation of Single Polyvinylidene Fluoride (PVDF) Composite Nanofibers, *Adv. Compos. Hybrid Mater.*, 2018, **1**(2), 332–340.

14 S. Sarkar, S. Garain, D. Mandal and K. K. Chattopadhyay, Electro-Active Phase Formation in PVDF-BiVO4 Flexible Nanocomposite Films for High Energy Density Storage Application, *RSC Adv.*, 2014, **4**(89), 48220–48227.

15 G. H. Kim, S. M. Hong and Y. Seo, Piezoelectric Properties of Poly(Vinylidene Fluoride) and Carbon Nanotube Blends: β-Phase Development, *Phys. Chem. Chem. Phys.*, 2009, **11**(44), 10506–10512.

16 M. El Achaby, F. Z. Arrakhiz, S. Vaudreuil, E. M. Essassi and A. Qaiss, Piezoelectric β-Polymorph Formation and Properties Enhancement in Graphene Oxide - PVDF Nanocomposite Films, *Appl. Surf. Sci.*, 2012, **258**(19), 7668–7677.

17 N. Soin, P. Zhao, K. Prashanthi, J. Chen, P. Ding, E. Zhou, T. Shah, S. C. Ray, C. Tsonos, T. Thundat, E. Siores and J. Luo, High Performance Triboelectric Nanogenerators Based on Phase-Inversion Piezoelectric Membranes of Poly(Vinylidene Fluoride)-Zinc Stannate (PVDF-ZnSnO3) and Polyamide-6 (PA6), *Nano Energy*, 2016, **30**(August), 470–480.

18 A. N. Arshad, M. H.-M. Wahid, M. Rusop, W. H.-A. Majid, R. H.-Y. Subban and M. D. Rozana, Dielectric and Structural Properties of Poly(Vinylidene Fluoride) (PVDF) and Poly(Vinylidene Fluoride-Trifluoroethylene) (PVDF-TrFE) Filled with Magnesium Oxide Nanofillers, *J. Nanomater.*, 2019, **2019**, 5961563.

19 A. Salimi and A. A. Yousefi, FTIR Studies of β-Phase Crystal Formation in Stretched PVDF Films, *Polym. Test.*, 2003, **22**(6), 699–704.

20 H. Luo, Y. Huang and D. Wang, The Crystallization and Crystal Transition of PVDF in PAN Nano-Tube, *Polymer*, 2013, **54**(17), 4710–4718.

21 R. Gregorio and E. M. Ueno, Effect of Crystalline Phase, Orientation and Temperature on the Dielectric Properties of Poly (Vinylidene Fluoride) (PVDF), *J. Mater. Sci.*, 1999, **34**(18), 4489–4500.

22 V. Sencadas, V. M. Moreira, S. Lanceros-Mendéz, A. S. Pouzada and R. Gregório, α - To - β Transformation on PVDF Films Obtained by Uniaxial Stretch, *Mater. Sci. Forum*, 2006, **514–516**(PART 2), 872–876.

23 N. Jahan, F. Mighri, D. Rodrigue and A. Ajji, Effect of the Inflation Strategy on the Piezoelectric Response of Cellular Poly(Vinylidene Fluoride) Ferroelectret, *J. Appl. Polym. Sci.*, 2019, **136**(20), 47540.

24 X. Ren, N. Meng, H. Zhang, J. Wu, I. Abrahams, H. Yan, E. Bilotti and M. J. Reece, Giant Energy Storage Density in PVDF with Internal Stress Engineered Polar Nanostructures, *Nano Energy*, 2020, **72**(February), 104662.

25 Z. X. Huang, M. M. Wang, Y. H. Feng and J. P. Qu, β-Phase Formation of Polyvinylidene Fluoride via Hot Pressing under Cyclic Pulsating Pressure, *Macromolecules*, 2020, **53**(19), 8494–8501.

26 H. Tao and J. Wu, New Poling Method for Piezoelectric Ceramics, *J. Mater. Chem. C*, 2017, **5**(7), 1601–1606.

27 H. Guo, C. Ma, X. Liu and X. Tan, Electrical Poling below Coercive Field for Large Piezoelectricity, *Appl. Phys. Lett.*, 2013, **102**(9), 6–10.

28 T. Granzow, A. B. Kounga, E. Aulbach and J. Rödel, Electromechanical Poling of Piezoelectrics, *Appl. Phys. Lett.*, 2006, **88**(25), 252907.
29 C. Ribeiro, D. M. Correia, S. Ribeiro, V. Sencadas, G. Botelho and S. Lanceros-Méndez, Piezoelectric Poly(Vinylidene Fluoride) Microstructure and Poling State in Active Tissue Engineering, *Eng. Life Sci.*, 2015, **15**(4), 351–356.
30 A. Kumar, V. V. Bhanu Prasad, K. C. James Raju and A. R. James, Optimization of Poling Parameters of Mechanically Processed PLZT 8/60/40 Ceramics Based on Dielectric and Piezoelectric Studies, *Eur. Phys. J. B*, 2015, **88**(11), 287–296.
31 E. Nilsson, A. Lund, C. Jonasson, C. Johansson and B. Hagström, Poling and Characterization of Piezoelectric Polymer Fibers for Use in Textile Sensors, *Sens. Actuators, A*, 2013, **201**, 477–486.
32 D. A. Porter, T. V.-T. Hoang and T. A. Berfield, Effects of In-Situ Poling and Process Parameters on Fused Filament Fabrication Printed PVDF Sheet Mechanical and Electrical Properties, *Addit. Manuf.*, 2017, **13**, 81–92.
33 H. Kim, F. Torres, Y. Wu, D. Villagran, Y. Lin and T.-L. Tseng, Integrated 3D Printing and Corona Poling Process of PVDF Piezoelectric Films for Pressure Sensor Application, *Smart Mater. Struct.*, 2017, **26**(8), 085027.
34 H. Cui, R. Hensleigh, D. Yao, D. Maurya, P. Kumar, M. G. Kang, S. Priya and X. Zheng, Three-Dimensional Printing of Piezoelectric Materials with Designed Anisotropy and Directional Response, *Nat. Mater.*, 2019, **18**(3), 234–241.
35 H. Kim, T. Fernando, M. Li, Y. Lin and T. L.-B. Tseng, Fabrication and Characterization of 3D Printed BaTiO3/PVDF Nanocomposites, *J. Compos. Mater.*, 2018, **52**(2), 197–206.
36 C. Lee and J. A. Tarbutton, Electric Poling-Assisted Additive Manufacturing Process for Lead-Free Piezoelectric Device Fabrication, *Procedia Manuf.*, 2015, **1**, 320–326.
37 H. Wei, X. Cauchy, I. O. Navas, Y. Abderrafai, K. Chizari, U. Sundararaj, Y. Liu, J. Leng and D. Therriault, Direct 3D Printing of Hybrid Nanofiber-Based Nanocomposites for Highly Conductive and Shape Memory Applications, *ACS Appl. Mater. Interfaces*, 2019, **11**(27), 24523–24532.
38 Q. Wu, S. Zou, F. P. Gosselin, D. Therriault and M. C. Heuzey, 3D Printing of a Self-Healing Nanocomposite for Stretchable Sensors, *J. Mater. Chem. C*, 2018, **6**(45), 12180–12186.
39 S. Zou, D. Therriault and F. P. Gosselin, Spiderweb-Inspired, Transparent, Impact-Absorbing Composite, *Cell Rep. Phys. Sci.*, 2020, **1**(11), 100240.
40 M. Ataur Rahman, B. C. Lee, D. T. Phan and G. S. Chung, Fabrication and Characterization of Highly Efficient Flexible Energy Harvesters Using PVDF-Graphene Nanocomposites, *Smart Mater. Struct.*, 2013, **22**(8), 085017.
41 A. Salimi and A. A. Yousefi, Conformational Changes and Phase Transformation Mechanisms in PVDF Solution-Cast Films, *J. Polym. Sci., Part B: Polym. Phys.*, 2004, **42**(18), 3487–3495.
42 E. Brunengo, M. Castellano, L. Conzatti, G. Canu, V. Buscaglia and P. Stagnaro, PVDF-Based Composites Containing PZT Particles: How Processing Affects the Final Properties, *J. Appl. Polym. Sci.*, 2020, **137**(20), 1–8.
43 J. Y. Lyu, S. Chen, W. He, X. X. Zhang, D. Y. Tang, P. J. Liu and Q. L. Yan, Fabrication of High-Performance Graphene Oxide Doped PVDF/CuO/Al Nanocomposites via Electrospinning, *Chem. Eng. J.*, 2019, **368**(November 2018), 129–137.
44 M. S. Sorayani Bafqi, R. Bagherzadeh and M. Latifi, Fabrication of Composite PVDF-ZnO Nanofiber Mats by Electrospinning for Energy Scavenging Application with Enhanced Efficiency, *J. Polym. Res.*, 2015, **22**(7), 1–9.
45 B. S. Lalia, E. Guillen-Burrieza, H. A. Arafat and R. Hashaikeh, Fabrication and Characterization of Polyvinylidenefluoride-Co-Hexafluoropropylene (PVDF-HFP) Electrospun Membranes for Direct Contact Membrane Distillation, *J. Membr. Sci.*, 2013, **428**, 104–115.
46 Commercial piezoelectric PVDF film. **https://piezopvdf.com/piezoelectric-poled-pvdf-film-d31/**.
47 H. Pei, Y. Xie, Y. Xiong, Q. Lv and Y. Chen, A Novel Polarization-Free 3D Printing Strategy for Fabrication of Poly (Vinylidene Fluoride) Based Nanocomposite Piezoelectric Energy Harvester, *Composites, Part B*, 2021, **225**(July), 109312.
48 X. Liu, Y. Shang, J. Zhang and C. Zhang, Ionic Liquid-Assisted 3D Printing of Self-Polarized β-PVDF for Flexible Piezoelectric Energy Harvesting, *ACS Appl. Mater. Interfaces*, 2021, **13**(12), 14334–14341.
49 P. H. Ducrot, I. Dufour and C. Ayela, Optimization of PVDF-TrFE Processing Conditions for the Fabrication of Organic MEMS Resonators, *Sci. Rep.*, 2016, **6**(January), 1–7.
50 B. Jaleh and A. Jabbari, Evaluation of Reduced Graphene Oxide/ZnO Effect on Properties of PVDF Nanocomposite Films, *Appl. Surf. Sci.*, 2014, **320**, 339–347.
51 J. X.-J. Zhang and K. Hosshino. *Molecular Sensors and Nanodevices*, 2014.
52 Building a Piezoelectric Generator. **https://www.Teachengineering.Org/Activities/View/Uoh_piezo_lesson01_activity1**.
53 J. Fu, Y. Hou, X. Gao, M. Zheng and M. Zhu, Highly Durable Piezoelectric Energy Harvester Based on a PVDF Flexible Nanocomposite Filled with Oriented BaTi2O5 Nanorods with High Power Density, *Nano Energy*, 2018, **52**(August), 391–401.
54 S. K. Karan, R. Bera, S. Paria, A. K. Das, S. Maiti, A. Maitra and B. B. Khatua, An Approach to Design Highly Durable Piezoelectric Nanogenerator Based on Self-Poled PVDF/AlO-RGO Flexible Nanocomposite with High Power Density and Energy Conversion Efficiency, *Adv. Energy Mater.*, 2016, **6**(20), 1–12.
55 B. Sun, X. Li, R. Zhao, H. Ji, J. Qiu, N. Zhang, D. He and C. Wang, Electrospun Poly(Vinylidene Fluoride)-Zinc Oxide Hierarchical Composite Fiber Membrane as Piezoelectric Acoustoelectric Nanogenerator, *J. Mater. Sci.*, 2019, **54**(3), 2754–2762.